SPECTRAL ANALYSIS OF THE TURBULENT ENERGY SPECTRUM IN SINGLE AND TWO-PHASE BUBBLY FLOWS IN DIFFERENT GEOMETRIES BASED ON DIRECT NUMERICAL SIMULATION RESULTS

C.S. Brown, I.A. Bolotnov
Department of Nuclear Engineering, North Carolina State University,
2500 Stinson Drive, Raleigh, NC, USA 27695-7909
csbrown3@ncsu.edu; igor_bolotnov@ncsu.edu

ABSTRACT

The spectral analysis of turbulent single and two-phase direct numerical simulation (DNS) data in flat plane channel, circular pipe, and reactor subchannel geometries is performed by using the recorded DNS velocity fluctuations as a function of time and applying the fast Fourier transformation (FFT). This results in an energy spectrum of the liquid turbulence in a frequency domain. The complexity of multiphase flows results in mixed velocity time history coming from either the liquid or gas phase. A modified single-phase signal that mimics the presence of bubbles ("pseudo-void") is developed to quantify the effect of the liquid signal intermittency as the bubble passes through a virtual probe.

Comparisons of single-phase, pseudo-void, and two-phase results quantify the changes to the expected -5/3 slope of the energy spectrum for single-phase flows due to turbulent interactions caused by the wakes behind a bubble. The two-phase energy spectra show a slope close to -3 while single-phase energy spectra exhibit the expected -5/3 slope in the different geometries. Pseudo-void results indicate that the change to the energy spectrum in bubbly two-phase flows is due entirely from liquid turbulence interactions with the bubble wakes.

A comprehensive spectral analysis for different geometries and different Reynolds number flows at varying distances from the wall is an essential step in developing physically sound closure models for bubble/liquid interactions. The comparison between different geometries demonstrates the direct applicability of various models to reactor-relevant geometries.

KEYWORDS
DNS, Energy spectrum, two-phase flow, spectral analysis

1. INTRODUCTION

Understanding the fundamental physics of multiphase flows is imperative in industries such as nuclear and chemical engineering. Safety and thermal-hydraulic analysis of current and future generations of nuclear reactors can benefit extensively from high fidelity predictive capabilities of multiphase flows. Computational multiphase fluid dynamics (CMFD) approach allows modeling three-dimensional distributions of gas/liquid volume fractions as well as mean velocities and turbulent parameters in various geometries. CMFD is more difficult than single-phase turbulence modeling since bubble interactions with the liquid turbulence must be modeled to achieve closure [1].

The one-dimensional energy spectrum of the velocity fluctuations in the liquid phase is essential in quantifying bubble/turbulence interactions [2]. The one-dimensional energy spectrum of the velocity fluctuations in the frequency domain can be calculated by performing fast Fourier transform (FFT) on the velocity fluctuations in the time domain. Advanced spectral turbulence models such as those of Bolotnov et al. [3] have shown that the energy spectrum of multiphase flows can improve turbulence closure terms and provide better predictions of flow characteristics. In single-phase flows, the -5/3 slope of the energy spectrum in the pure inertial subrange is known from Kolmogorov theory. However, the slope of the energy spectrum for multiphase flows is not so well understood and differing values are found in the literature.

The majority of available data for the evaluation of the slope of the energy spectrum in multiphase flows, both experimental and numerical, exists for purely bubble-induced turbulence. Bubble induced turbulence (pseudo-turbulence) refers to an initially at rest flow that is forced by rising bubbles as the only source of liquid turbulence energy [4]. Lance and Bataille [5] suggested the ratio of bubble-induced kinetic energy to the turbulent kinetic energy in the absence of bubbles as an appropriate parameter to characterize a bubbly flow. Rensen et al. [6] defined this dimensionless quantity as the "bubblance" parameter (*b)* and showed that $b=\infty$ for pure pseudo-turbulence and suggested that the slope of the energy spectrum can be determined from the bubblance alone. Although the bubblance parameter is useful for characterizing a bubbly flow it has not been successful as the only determinant of the slope of the energy spectrum [2, 7]. Sathe et al. [7] suggested that circulation velocity, bubble size distribution, and lateral variation of mean bubble size in an experimental bubble column greatly affect the energy spectrum.

Experimental techniques such as particle image velocimetry (PIV) and hot wire anemometry (HWA) have been used to evaluate the liquid energy spectrum in pseudo-turbulent bubbly flows. Lance and Bataille [5] found the classical -5/3 power law gradually replaced by a -8/3 slope in the high frequency range as void fraction was increased in bubbly turbulence and these results were reproduced by Wang et al. [1]. Rensen et al. [6] was not able to reproduce these results and instead reported a slope slightly less than -5/3 and attribute their differences to the bubblance parameter. Shawkat et al. [8] experimentally investigated the energy spectrum of air-water flow in a vertical pipe and found slopes ranging from -8/3 to -10/3 dependent on the void fraction. They proposed that the traditional inertial subrange might not be valid for two-phase bubbly flows since there is energy production due to liquid-bubble interactions at the traditional inertial subrange length scales. Bolotnov et al. [9] made similar arguments that bubble contributions to the liquid turbulence occur at length scales on the order of the bubble diameter in their spectral cascade-transport model development. Mercado et al. [10] found a slope of -3.18 for the energy spectrum with no dependency on the void fraction. Mendez-Diaz et al. [11] experimentally analyzed pseudo-turbulent flow for two different bubble sizes and three different viscosity liquids and found a slope close to -3 for all cases. A slope of -5/3 transitioning to -3 at higher wave numbers was reported by Sathe et al. [7].

Numerical experiments are a particularly powerful tool that complement and provide comparisons to experimental results. Sugiyama et al. [12] modeled 800 rising particles as bubbles for pseudo-turbulent flow and also found a -3 slope. Mazzitelli and Lohse [4] simulated 288000 microbubbles for pseudo-turbulence but did not resolve the bubble wakes. They report a -5/3 slope consistent with their observation that the -3 slope is due to energy deposited by the bubble wake that is then directly dissipated. Roghair et al. [13] reported a slope of -3 in DNS of pseudo-turbulent flow for a converged case with 5% void fraction as well as a -3 slope for a non-fully converged case with 15% void fraction. Riboux et al. [14] also proposed that bubble-induced agitation of the liquid phase mainly results from wake interactions and found a slope of -3. They modeled the bubbles as fixed momentum sources and reproduced the wake some distance from the bubble to minimize computational cost. The increasing capabilities of high performance super-computing continue to expand DNS capabilities by allowing simulations of higher Reynolds numbers, larger domain sizes, and more complex geometries. Bolotnov [15] used PHASTA to

fully resolve 60 bubbles in a turbulent flow with a Reynolds number based on friction velocity of 400. Fang et al. [16] have used PHASTA to simulate turbulent single-phase flow, as well as turbulent bubbly two-phase flow, in reactor subchannel geometry. Analytic considerations have also shown a -3 scaling of the energy spectrum for two-phase bubbly flows (e.g. [5], [9], [17]).

Estimating the two-phase energy spectrum has additional challenges since the complexity of two-phase flows results in a time history of mixed velocity signals coming from either the liquid or gas phase. The liquid phase velocity history is discontinuous due to the passage of a bubble over an experimental or numerical probe. There exist several methods of handling the discontinuous liquid velocity signal so that FFT can be applied to calculate the energy spectrum although none of these methods have been shown to be definitive. Ilic et al. [2] compared four different methods of bridging the gap in the liquid velocity signal: (1) the method of Tsuji and Morikawa [18] to replace the defective part of the signal with a linear interpolation, (2) the method of Gherson and Lykoudis [19] to patch together the successive liquid velocity signal, (3) the method of Wang et al. [1] to replace the defective parts of the signal with the mean velocity of the liquid phase, and (4) the method of Panidis and Papailiou [20] to analytically replace the defective part of the signal with segments having the same statistical properties of the liquid signal. Ilic et al. [2] found the method of replacing the defective parts of the signal with the mean velocity of the liquid phase to be most promising. Shawkat et al. [8] also compared different methods of bridging over the defective parts of the liquid velocity signal and chose to use the linear interpolation method. Mercado et al. [10] and Roghair et al. [13] chose to calculate the energy spectrum using the liquid pieces between the passage of bubbles and then average for the energy spectrum. This approach creates issues since the length of each data segment will not be the same. Using data segments of differing lengths required the calculation of a minimum data segment length to be included in the averaging for the energy spectrum. Note that even with a minimum segment length the amount of data will decrease with increasing void fraction and the resolved frequency range will be dissimilar for differing data length segments.

Although pseudo-turbulent flows provide valuable insight into the slope of the energy spectrum in multiphase flows, the conditions of multiphase flow in nuclear reactor subchannels are highly turbulent and CMFD approach must capture the physics of the multiphase energy spectrum for turbulent conditions. Mercado et al. [10] expressed interest in flows where turbulent effects become dominant. Mendez-Diaz et al. [11] recently stated that calculating the energy spectrum in fully turbulent flow could demonstrate whether the spatial inhomogeneity of bubbles or the normal turbulent energy cascade dominates the shape of the energy spectrum.

In the present work, turbulent DNS data in flat plane channel, reactor subchannel, and circular pipe geometries are spectrally analyzed for both single and two-phase bubbly flow. We develop a modified single-phase signal (which we call “pseudo-void”) to mimic the presence of bubbles to show that bubble interactions with the liquid turbulence are due to contributions from the bubble wake. Spectrally analyzing turbulent single and bubbly two-phase flows in different geometries provides high quality data for the literature and increases capabilities of advanced turbulence models.

2. NUMERICAL METHOD

Single and two-phase DNS (Table I) of fully-developed turbulent flow were performed [15, 16] using PHASTA where the liquid/gas interface was tracked using a level-set method for two-phase simulations. DNS for the circular pipe geometry are currently being performed in-house and being spectrally analyzed as data becomes available. Details about the numerical method and capabilities of the PHASTA code can be found in [15]. During each PHASTA simulation (Figure 1) instantaneous flow quantities (i.e. velocity, pressure, etc.) were recorded at specific locations within the computational domain called virtual probes. These virtual probes were placed at planar locations normal to the flow-direction covering different distances from the wall. At each particular wall distance, virtual probes were also placed in the span-wise

direction to increase the statistical sample. For example, the left side of Figure 2 shows how the virtual probes are arranged for the subchannel simulations performed by Fang et al. [16]. The amount of DNS time considered can be described by the Large Eddy TurnOver Time (LETOT) [21] defined as one-half the hydraulic diameter divided by the friction velocity.

Recording instantaneous flow quantities at each time-step in a PHASTA simulation results in a discrete time velocity signal characterized by random turbulence induced fluctuations. By applying Reynolds decomposition [22], the instantaneous velocity signal u_i is decomposed into its mean U_i and fluctuating components u_i' ($u_i = U_i + u_i'$). The mean velocity component is the time-average of the instantaneous velocity over the simulation time and the fluctuating velocity components are then calculated for each discrete time in the simulation.

The phase indicator function denotes the presence of a bubble at a virtual probe in two-phase simulations and thus defines defective temporal locations of the liquid velocity signal. Following Shawkat et al. [8], we have used the linear interpolation technique for replacing the defective parts of the velocity signal since our comparisons of replacing the signal with the mean liquid velocity have also shown bias in the spectra at the high frequency range. The right side of Figure 2 shows both fluctuating velocity signals calculated from DNS using the mean insertion method and the linear interpolation method where the bubble locations are denoted below the velocity signal.

Table I. A summary of the parameters for DNS data spectrally analyzed in this paper.

Parameter	Plane Channel [15]		Circular Pipe			Subchannel [16]	
	Single-Phase	Two-Phase	Single-Phase	Two-Phase	Two-Phase	Single-Phase	Two-Phase
Reynolds number based on friction velocity, Re_τ	400	400	1920	1920	1920	400	996
Mesh size, elements	20M	20M	1,900M	240M	1,900M	52M	1,000M
Number of bubbles	0	60	0	112	895	0	262
Void fraction, α	0%	1%	0%	1%	1%	0	1%
Bubble diameter (wall units), d^+	N/A	81.2	N/A	288	144	N/A	200
Eotvos number, $Eo = \frac{(\rho_l - \rho_g) g d^2}{\sigma}$		0.110		0.56	1.31		2.44
Morton number, $Mo = \frac{g\mu_l^4(\rho_l - \rho_g)}{\rho_l^2 \sigma^3}$		1.33×10^{-11}		4.13×10^{-14}	1.25×10^{-12}		5.1×10^{-13}
Weber number, $We = \frac{\rho_l u_R^2 d}{\sigma}$		0.367		3.0	4.21		0.69

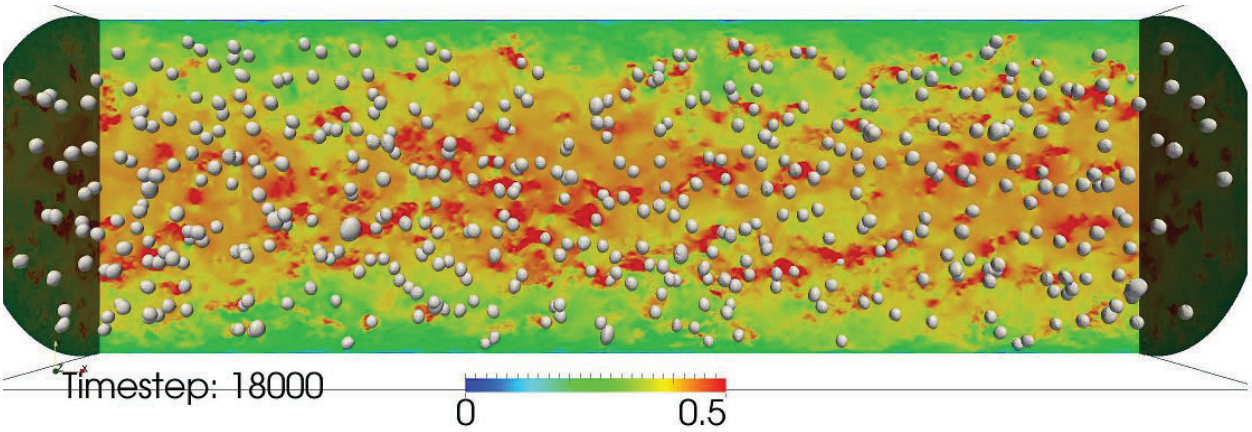

Figure 1. Instantaneous velocity distribution of a two-phase PHASTA simulation performed for the circular pipe geometry with 895 bubbles.

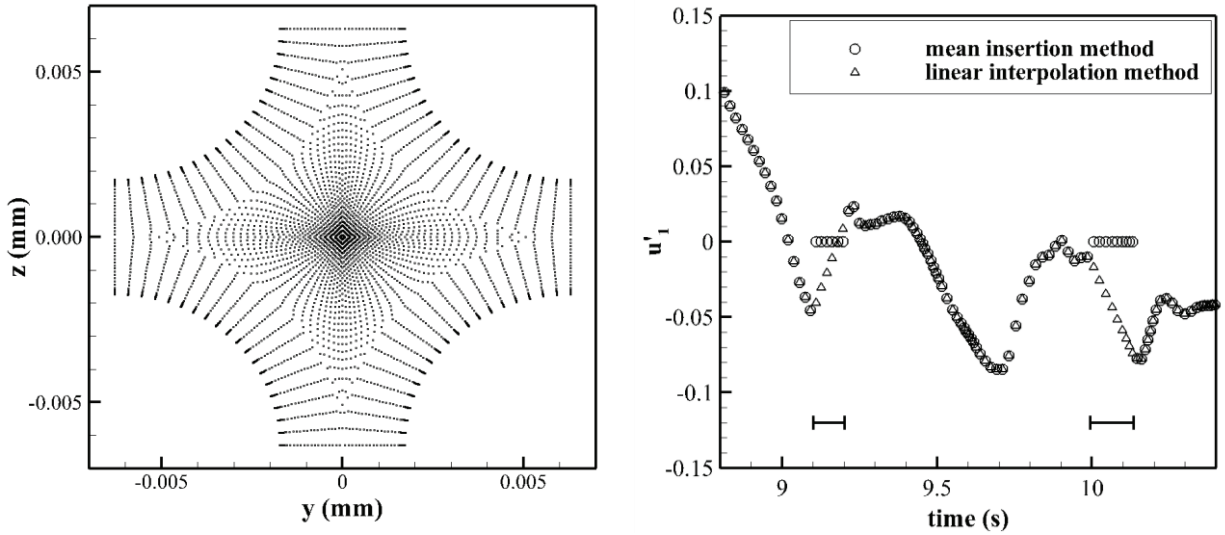

Figure 2. Left: Virtual probe locations in the PHASTA simulations performed by Fang et al. [16] of a single reactor subchannel. Right: The fluctuating velocity signal at a particular span-wise direction for every eighth time step with the defective portions replaced by the mean liquid velocity (circles) and a linear interpolation over the defective time (triangles) with bubbles (closed lines) at about 9.1 seconds and 10 seconds.

Just as Riboux et al. [14] we believe that the bubble effects on the energy spectrum are due to bubble wake interactions with the liquid turbulence. We formulate pseudo-void numerical experiments to show that bubble/turbulence interactions change the slope of the energy spectrum only when the bubble wakes are present. Shawkat et al. [8] compared different methods for bridging the gap in the defective two-phase velocity signal by electronically interrupting a single-phase signal with the gas identifier signal from a two-phase signal. Following this approach, pseudo-void simulations were developed where the phase indicator signal from two-phase DNS is overlaid on the velocity signal of single-phase DNS, mimicking the presence of bubbles in the data. The single-phase data is interrupted due to the mimicked gas phase but does contain the bubble wakes since the velocity signal is not altered outside of the prescribed defective portions. The linear interpolation technique was used to bridge the defective parts of the pseudo-void signal.

The velocity fluctuations at each time step were used to compute the single-point velocity correlation (1) and FFT was then applied to calculate the turbulent kinetic energy spectrum in the frequency domain using Bartlett's method [23]. In a similar approach to Roghair et al. [13], who averaged the energy spectrum over 27 probes, the energy spectrum was calculated for each of the span-wise virtual probes at a particular wall distance and then averaged.

$$R_{ii}(t_j) = \frac{1}{2} u_i'(t_j) u_i{}'(t_j) \tag{1}$$

3. RESULTS

3.1 Plane Channel

It is necessary to use enough data points in the averaging window when performing FFT to calculate the energy spectrum. Comparisons of the energy spectrum for different numbers of points as integer powers of 2 for the plane channel geometry have shown that using as few as 256 points in the averaging window had minimum deviations from much larger window widths. The DNS data must be statistically steady-state before being spectrally analyzed and the left side of Figure 3 shows that the behavior of the single-phase energy spectra is similar for each of the 42 virtual probes in the plane channel case. Similar or better behavior at each of the virtual probes was observed for all of the cases presented here.

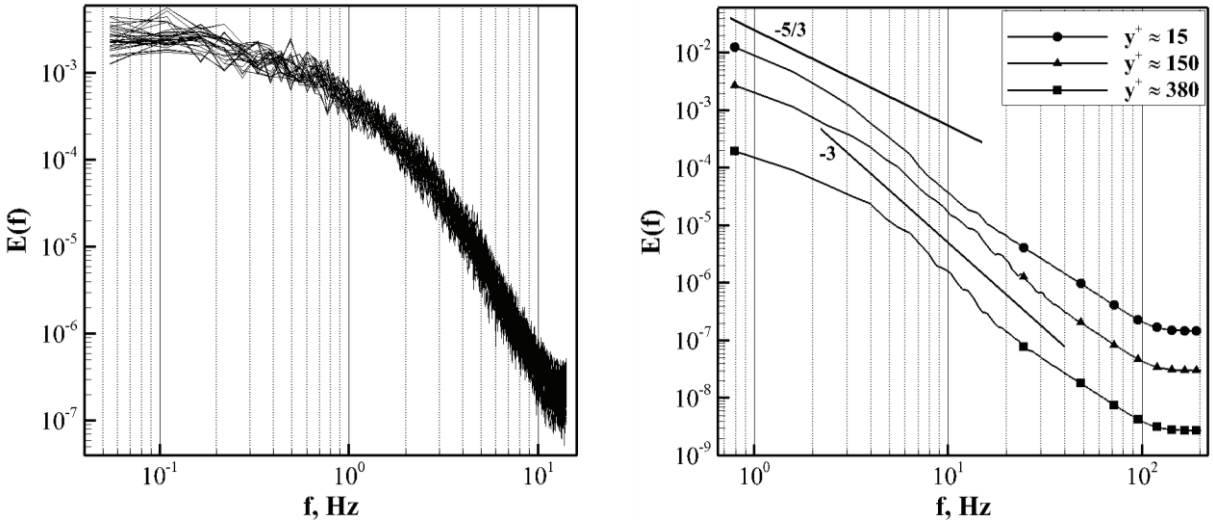

Figure 3. Left: The energy spectra for each of the 42 span-wise locations in the single-phase plane channel simulation at y^+≈15. Right: Energy spectra for the two-phase plane channel simulations at y^+≈380 (squares), y^+≈150 (triangles), and y^+≈15 (circles).

For the two-phase plane channel simulations, 15 averaging windows each with a width of 512 points were used for a total simulation time slightly greater than 4 LETOTs. The right side of Figure 3 shows the energy spectra for the two-phase plane channel simulations at three different y^+ locations. Note the difference in energy magnitudes since more energy is present in the energy producing region close to the wall. The energy spectra have a slope close to -3 over a frequency range of slightly less than two decades. The flattened profile in the high frequency range is interesting and is due to oversampling the DNS data which causes very high frequency results in the energy spectra at frequencies higher than the Kolmogorov scales of interest. Similar spectral shapes have been shown by Mercado et al. [10] and Roghair et al. [13].

In contrast to the suggestions of Rensen et al. [6], the bubblance is much less than 1 in the turbulent DNS results presented here but the -3 scaling of the slope in the energy spectrum is still observed.

Single-phase plane channel simulations were spectrally analyzed with 16 averaging windows each with a width of 512 points for a total simulation time of about 63 LETOTs. The much longer simulation time is a result of the larger time step of the single-phase DNS compared to two-phase DNS. Therefore, to properly implement the pseudo-void techniques the amount of single-phase simulation time used had to be consistent with the overall time of the two-phase record so that bubble locations could be projected onto the single-phase data. The left side of Figure 4 shows how bubbles are distributed at each span-wise location over time for $y^+ \approx 150$ in the two-phase plane channel simulation. A single FFT averaging window with a length of 534 points was used for the pseudo-void spectral analysis so that the time was also about 4 LETOTs. The right side of Figure 4 shows comparisons for bubble contributions at each span-wise location for two-phase and pseudo-void calculations, where the bubble contribution is the number of bubbles at a span-wise direction normalized by the total bubbles in the simulation. Clearly, we are projecting the two-phase bubble distribution quite well onto the single-phase DNS data. There are some discrepancies since the larger time step in these single-phase simulations may not resolve bubbles measured by a virtual probe in two-phase simulations for a very short time span.

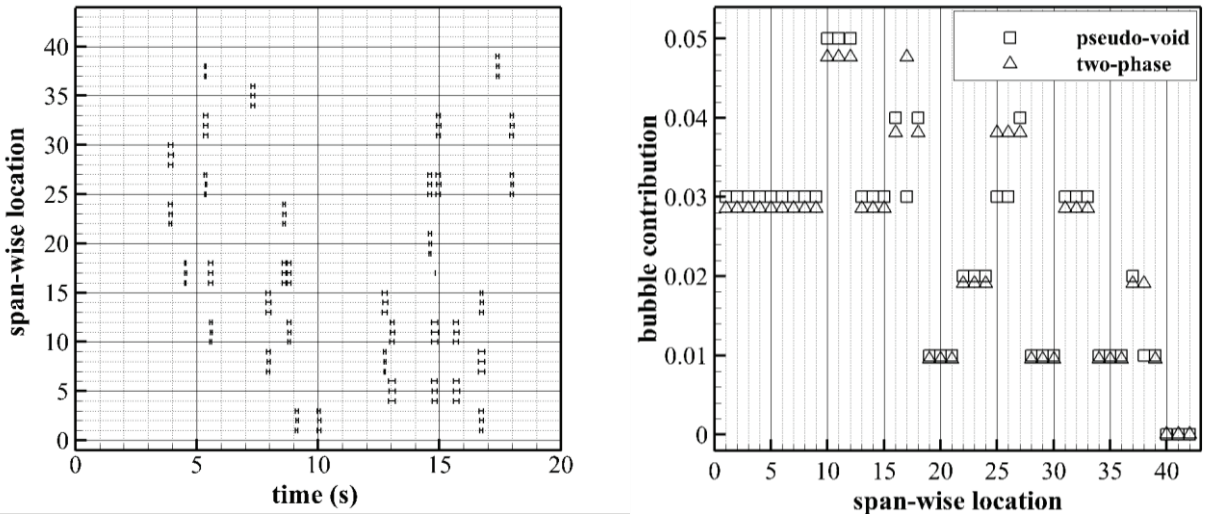

Figure 4. Left: Bubble locations (closed-end lines) in time at each of the span-wise virtual probes for the two-phase plane channel case (y+≈150). Right: Bubble contributions from each span-wise location to the overall number of bubbles present in the flow for $y^+ \approx 150$.

Figure 5 shows the single-phase and pseudo-void spectra, as well as a single-phase spectrum for the same time length as the pseudo-void simulation, for three different y^+ locations. Note the vertical axis is different since more energy is present in the energy producing range close to the wall. The expected -5/3 slope is evident and we have also labeled the steeper slope in the higher frequency range. The pseudo-void results show no difference from the single-phase data, demonstrating that the change of the energy spectrum slope in the two-phase simulations is due to bubble wake interactions with the liquid turbulence. The energy spectra for shorter times (pseudo-void, single-phase with pseudo void time) are not as smooth as the energy spectra for the full single-phase data length since only one FFT averaging window had to be used.

As proposed by Mazzitelli and Lohse [4], energy produced by a bubble wake is deposited and immediately dissipated. This occurs at length scales similar to the bubble diameter and within the pure

inertial subrange in single-phase flows. Therefore, the modification to the energy spectrum slope in two-phase flows is similar to the dissipation range in single-phase flows since contributions to the energy spectrum by dissipating bubble wakes dominates.

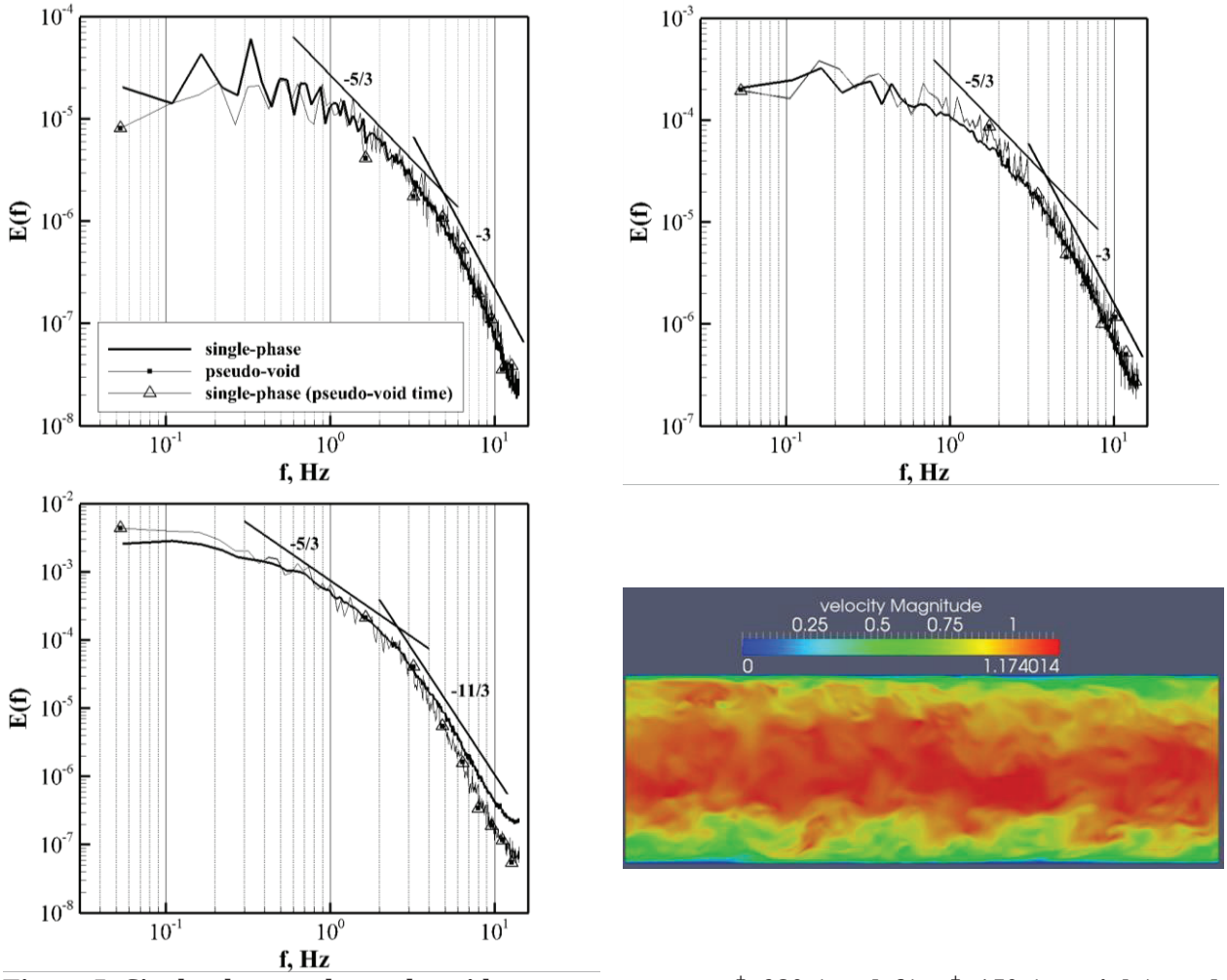

Figure 5. Single-phase and pseudo-void energy spectra at y^+≈380 (top left), y^+≈150 (top right), and y^+≈15 (bottom left) for the plane channel geometry. The full simulation time of about 292 seconds is indicated by the thick line, the pseudo-void simulation is indicated by the squares, and a single-phase simulation for the same simulation time as the pseudo-void simulation is indicated by the triangles. Also shown is a snapshot of the instantaneous velocity distribution for the single-phase plane channel DNS (bottom right).

3.2 Pipe Geometry

3.2.1 112 Bubble case

Spectral analysis for the circular pipe geometry with 112 bubbles was performed using the currently available DNS data. Two-phase analysis was performed with 9 averaging windows of 1024 points each for a total simulation time of about 0.5 LETOT. Due to the much smaller time step of these simulations in comparison to the plane channel geometry more points were required per averaging window. The left side of Figure 6 shows the energy spectra for the two-phase circular pipe simulations at three different y^+ locations where again the difference in spectrum magnitudes is due to the energy producing region close

to the wall. The two-phase energy spectra in the circular pipe geometry also exhibit a slope close to -3 over a frequency range of as much as two decades. The right side of Figure 6 shows a cross-sectional snapshot of the DNS velocity distribution for the circular pipe with 112 bubbles.

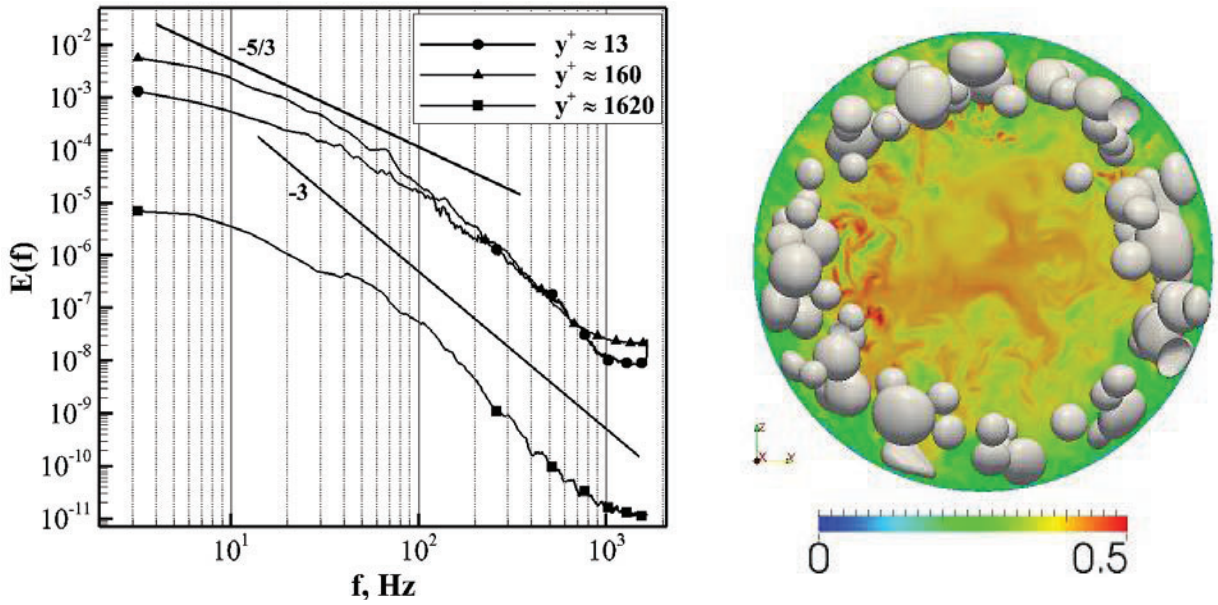

Figure 6. Left: Energy spectra for the two-phase circular pipe simulations with 112 bubbles at y+≈1620 (squares), y+≈160 (triangles), and y+≈13 (circles). Right: Snapshot of the instantaneous velocity distribution for the 112 bubble circular pipe DNS.

Single-phase and pseudo-void analyses were performed with averaging windows of 1024 points each for a total simulation time of about 0.36 LETOT. Since the time steps were similar for the single-phase and two-phase DNS of the circular pipe the bubble contributions were nearly identical for each span-wise direction. Figure 7 shows the single-phase and pseudo-void energy spectra for the circular pipe geometry as well as DNS results for the velocity distribution inside the pipe at a particular time step. As with the plane channel geometry, note the vertical axis is different in the spectra plots since more energy is present in the energy producing range close to the wall. The expected -5/3 slope is shown in the results and there is a transition to a steeper slope at higher frequencies. The pseudo-void results again show no difference from the single-phase data and demonstrate that the change of the energy spectrum slope in multiphase flows is due to the bubble wake interactions with the liquid turbulence.

3.2.2 895 Bubble case

Available two-phase data for the circular pipe geometry with 895 bubbles was also spectrally analyzed and results are shown in Figure 8. Due to limited data availability, 3 averaging windows of 1024 points were used for a total simulation time of about 0.13 LETOT for this case. Note that the energy spectrum is not higher closer to the wall in this case since preliminary data may not have fully developed the wall-peaked void fraction profile and bubbles present in the center of the channel induce turbulence. However, the available two-phase data with 895 bubbles also indicates a -3 scaling of the energy spectrum.

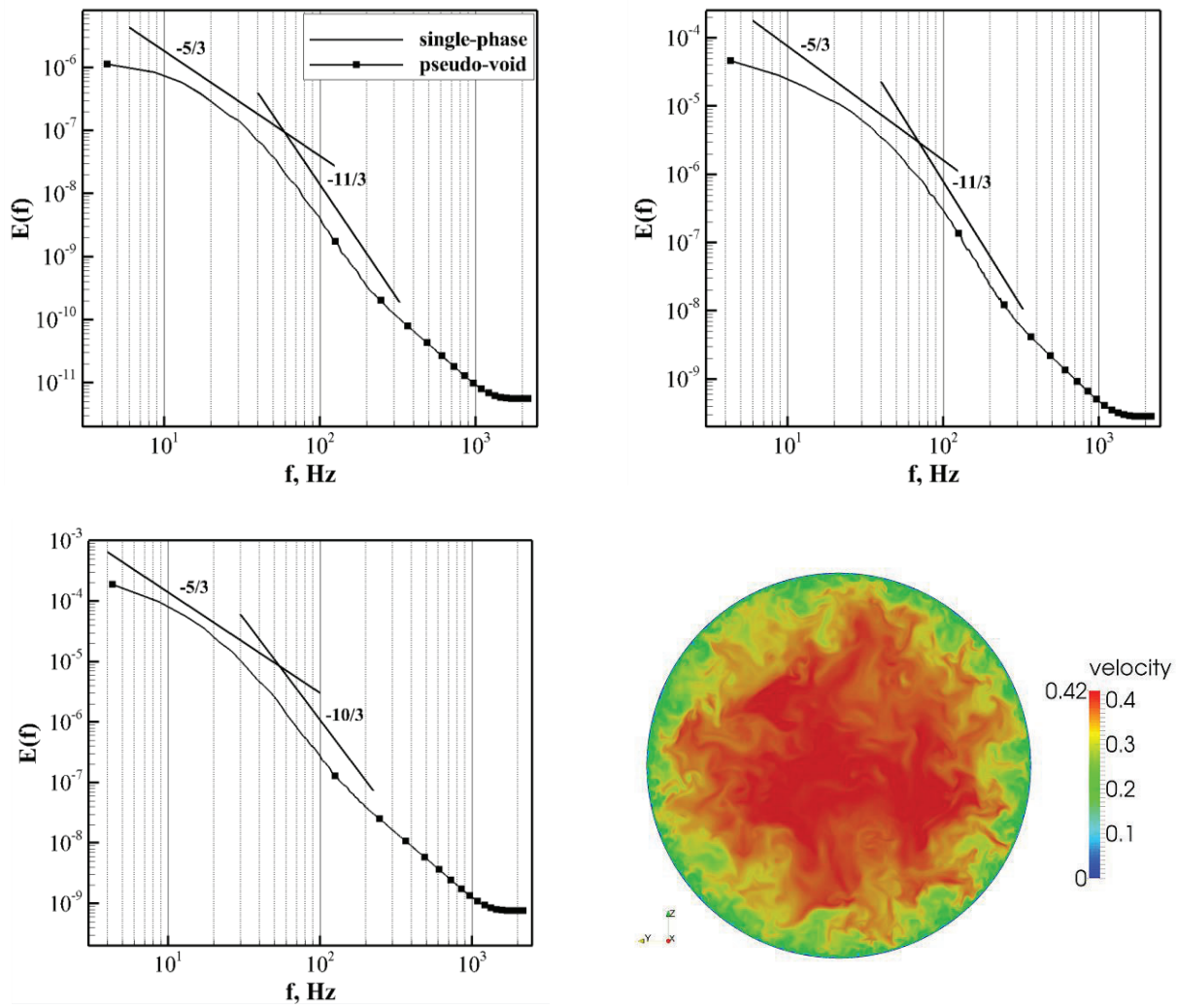

Figure 7. Single-phase (solid line) and pseudo-void (solid line with squares) energy spectra for the circular pipe at y+≈1620 (top left), y+≈160 (top right), and y+≈13 (bottom left). Also shown is a radial snapshot of the instantaneous velocity distribution for the single-phase circular pipe DNS (bottom right).

3.3 Subchannel Geometry

Spectral analysis of the single-phase subchannel was performed using 19 windows of 2048 points for a total data time of about 6.3 LETOTs. The energy spectra at different y^+ locations are shown on the left side of Figure 9 and the expected -5/3 scaling in the inertial subrange is represented in the single-phase data. The y^+ locations are formulated differently than for traditional channel flow [16] but still represent distance to the wall (the fuel pins in the subchannel case). Again the steeper slope in the dissipation range at the higher frequencies varies somewhat depending on wall distance but is close to -3.

Turbulent two-phase bubbly flow DNS for this subchannel geometry with 262 bubbles is currently being performed by Fang et al. [16] and will continue to be spectrally analyzed as the data becomes available. Current spectral results with 2 averaging windows of 950 points for about 0.08 LETOT (right side of Figure 9) show the -3 scaling even for the limited amount of data.

3.4 Comparison of Geometries

A direct comparison of the two-phase energy spectra for all of the considered geometries in this work is presented in Figure 10 for y^+ values of about 150. The energy spectrum for each of the geometries is normalized such that the maximum frequency value is 1. Similar shapes, with a power law scaling close to -3, are evident for each of the considered geometries.

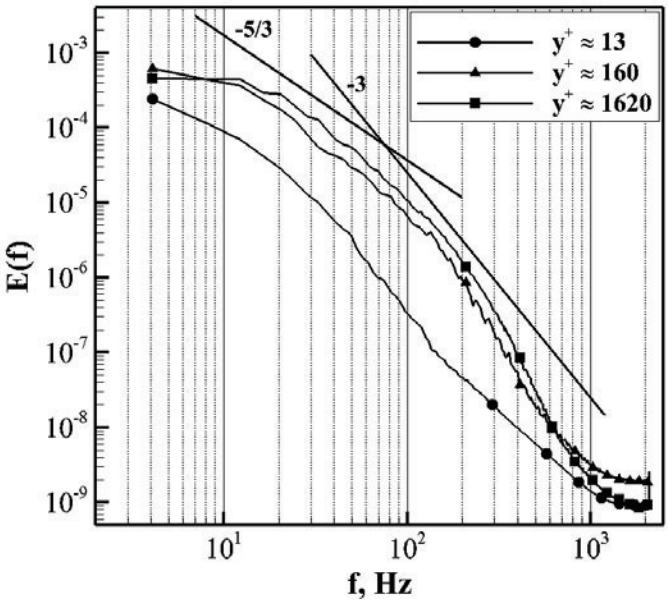

Figure 8. Energy spectra for the two-phase circular pipe simulations with 895 bubbles at y+≈1620 (squares), y+≈160 (triangles), and y+≈13 (circles).

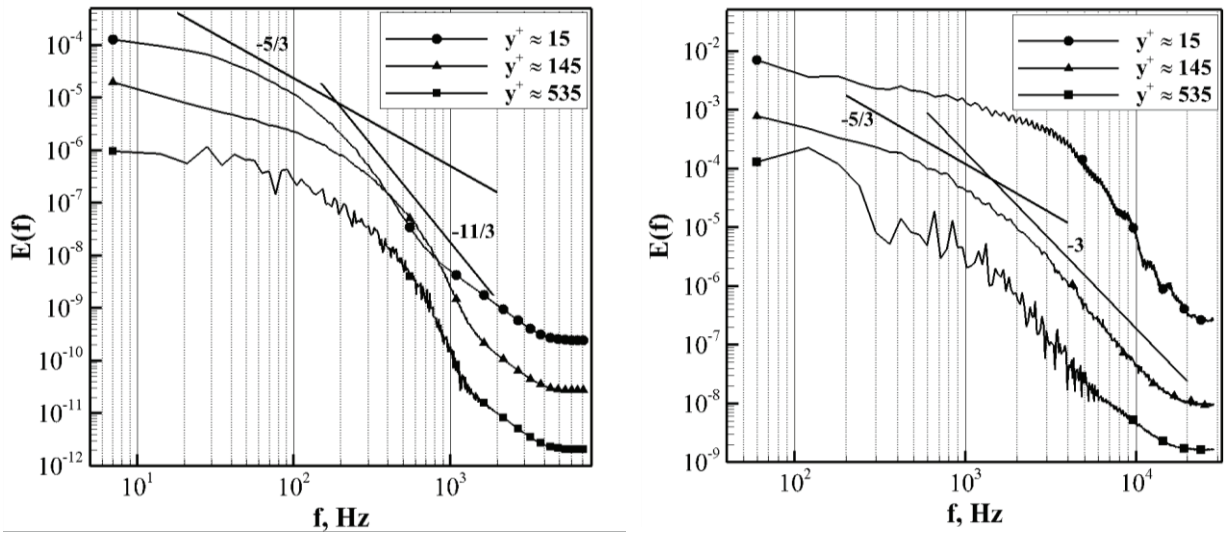

Figure 9. Energy spectra for the subchannel geometry at y+≈535 (squares), y+≈145 (triangles), and y+≈15 (circles) for single-phase DNS (left) and two-phase DNS with 262 bubbles (right).

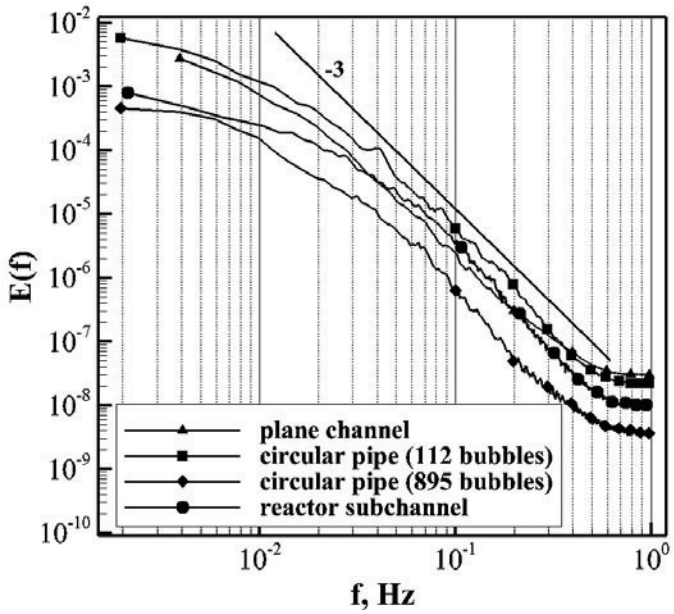

Figure 10. Comparison of the energy spectra for all of the two-phase simulations in each of the geometries considered in the current work.

4. CONCLUSIONS

Results from turbulent single and two-phase bubbly DNS in different geometries [15, 16] have been spectrally analyzed. We have shown that the energy spectrum has a power law scaling close to -3 for turbulent bubbly two-phase flow, which agrees with experiments and analytic considerations. The new pseudo-void technique has further indicated that the scaling of the energy spectrum in bubbly two-phase flow is due entirely to liquid/turbulence interactions with the bubble wakes. Mazzitelli and Lohse [4] presented similar conclusions when bubble wakes were not resolved in DNS. The spectral analysis of turbulent DNS data for reactor subchannel and circular pipe geometries have shown the traditional -5/3 power law for single-phase flow. The slope of the dissipation range in single-phase flows is close to -3 and indicates why this scaling is present in two-phase flows where the bubble wakes are dissipating at scales in the traditional pure inertial subrange.

Spectrally analyzing DNS for turbulent flows in different geometries provides more data on the scaling of the energy spectrum and improves turbulence closure modeling. The current work indicates that the shape of the energy spectrum for two-phase bubbly flows is consistent for different geometries. Quantifying the contributions of the bubble wakes to particular frequency/wavenumber ranges will expand CMFD capabilities to properly handle bubble effects on the liquid turbulence. The use of high fidelity CMFD simulations with a more physically derived background provides confidence in reactor safety calculations.

As computational capabilities continue to increase comparisons of the energy spectrum for differing void fractions in turbulent flow, such as those that Riboux et al. [14] conducted for pseudo-turbulence, will be conducted. In response to Mendez-Diaz et al. [11], we conclude that the spatial inhomogeneity of bubbles dominates the shape of the energy spectrum in bubbly two-phase turbulence. The -3 scaling of the energy spectrum is present in the turbulent cases considered although the bubblance is much less than 1.

ACKNOWLEDGEMENTS

The authors would like to acknowledge the support from Consortium for Advanced Simulation of Light Water Reactors (http://www.casl.gov), an Energy Innovation Hub (http://www.energy.gov/hubs) for Modeling and Simulation of Nuclear Reactors under U.S. Department of Energy [grant number DE-AC05-00OR22725]. An award of computer time was provided by the ASCR Leadership Computing Challenge (ALCC) program. This research used resources of the Argonne Leadership Computing Facility, which is a DOE Office of Science User Facility supported under Contract DE-AC02-06CH11357. The DNS solutions presented herein made use of the Acusim linear algebra solution library provided by Altair Engineering Inc. along with the meshing and geometric modelling libraries developed by Simmetrix Inc. The authors would like to thank Jun Fang for his assistance with the subchannel geometry.

REFERENCES

1. Wang, S. K., Lee, S. J., Jones, O. C. & Lahey, R. T. Statistical-Analysis of Turbulent 2-Phase Pipe-Flow. *Journal of Fluids Engineering-Transactions of the Asme* **112**, 89-95 (1990).
2. Ilic, M., Worner, M. & Cacuci, D. G. *Evaluation of energy spectra in bubble driven liquid flows from direct numerical simulations* (6th International Conference on Multiphase Flow, ICMF 2007, Leipzig, Germany, 2007).
3. Bolotnov, I. A., Lahey, R. T., Drew, D. A., Jansen, K. E. & Oberai, A. A. Spectral cascade modeling of turbulent flow in a channel. *Japanese Journal of Multiphase Flow* **23**, 190-204 (2009).
4. Mazzitelli, I. M. & Lohse, D. Evolution of energy in flow driven by rising bubbles. *Physical Review E* **79** (2009).
5. Lance, M. & Bataille, J. Turbulence in the Liquid-Phase of a Uniform Bubbly Air Water-Flow. *J. Fluid Mech.* **222**, 95-118 (1991).
6. Rensen, J., Luther, S. & Lohse, D. The effect of bubbles on developed turbulence. *J. Fluid Mech.* **538**, 153-187 (2005).
7. Sathe, M., Joshi, J. & Evans, G. Characterization of turbulence in rectangular bubble column. *Chemical Engineering Science* **100**, 52-68 (2013).
8. Shawkat, M. E., Ching, C. Y. & Shoukri, M. On the liquid turbulence energy spectra in two-phase bubbly flow in a large diameter vertical pipe. *Int. J. Multiphase Flow* **33**, 300-316 (2007).
9. Bolotnov, I. A., Lahey, R. T.,Jr., Drew, D. A. & Jansen, K. E. Turbulent cascade modeling of single and bubbly two-phase turbulent flows. *Int. J. Multiphase Flow* **34**, 1142-1151 (2008).
10. Mercado, J. M., Gomez, D. C., Van Gils, D., Sun, C. & Lohse, D. On bubble clustering and energy spectra in pseudo-turbulence. *J. Fluid Mech.* **650**, 287-306 (2010).
11. Mendez-Diaz, S., Serrano-Garcia, J. C., Zenit, R. & Hernandez-Cordero, J. A. Power spectral distributions of pseudo-turbulent bubbly flows. *Phys. Fluids* **25**, 043303 (2013).
12. Sugiyama, K., Takagi, S. & Matsumoto, Y. Multi-scale analysis of bubbly flows. *Comput. Methods Appl. Mech. Eng.* **191**, 689-704 (2001).
13. Roghair, I. *et al*. Energy spectra and bubble velocity distributions in pseudo-turbulence: Numerical simulations vs. experiments. *Int. J. Multiphase Flow* **37**, 1093-1098 (2011).
14. Riboux, G., Legendre, D. & Risso, F. A model of bubble-induced turbulence based on large-scale wake interactions. *J. Fluid Mech.* **719**, 362-387 (2013).
15. Bolotnov, I. A. Influence of Bubbles on the Turbulence Anisotropy. *Journal of Fluids Engineering-Transactions of the Asme* **135**, 051301 (2013).
16. Fang, J., Rasquin, M. & Bolotnov, I. A. *Interface tracking simulations of bubbly flows in the PWR relevant geometries*, NURETH-16, Chicago, IL, USA, 2015).
17. Risso, F. Theoretical model for k(-3) spectra in dispersed multiphase flows. *Phys. Fluids* **23**, 011701 (2011).
18. Tsuji, Y. & Morikawa, Y. Ldv Measurements of an Air Solid 2-Phase Flow in a Horizontal Pipe. *J. Fluid Mech.* **120**, 385-409 (1982).

19. Gherson, P. & Lykoudis, P. S. Local Measurements in 2-Phase Liquid-Metal Magneto-Fluid-Mechanic Flow. *J. Fluid Mech.* **147**, 81-104 (1984).
20. Panidis, T. & Papailiou, D. D. The structure of two-phase grid turbulence in a rectangular channel: an experimental study. *Int. J. Multiphase Flow* **26**, 1369-1400 (2000).
21. Di Liberto, M. & Ciofalo, M. A study of turbulent heat transfer in curved pipes by numerical simulation. *Int. J. Heat Mass Transfer* **59**, 112-125 (2013).
22. Pope, S. B. in *Turbulent flows* (Cambridge University Press, Cambridge ;New York, 2000).
23. Proakis, J. G. in *Digital signal processing : principles, algorithms, and applications* (ed Manolakis, D. G.) (Prentice Hall, Englewood Cliffs, NJ., 1996).